Dalton Transactions

Ternary Alkali ion Thiogallates, A5GaS4 (A = Li and Na) with Isolated Tetrahedral Building Units and Their Ionic conductivity

Journal:	*Dalton Transactions*
Manuscript ID	DT-ART-03-2021-000766.R1
Article Type:	Paper
Date Submitted by the Author:	07-Apr-2021
Complete List of Authors:	Balijapelly, srikanth; Missouri University of Science and Technology, Chemistry Sandineni, Prashanth; Missouri University of Science and Technology, Chemistry; Missouri University of Science and Technology, Chemistry Adhikary, Amit; IISER Bhopal, ; Gerasimchuk, Nikolay; Missouri State University, Department of Chemistry Chernatynskiy, Aleksandr; Missouri University of Science and Technology, Physics Choudhury, Amitava; Missouri University of Science and Technology, Chemistry

SCHOLARONE™
Manuscripts

Please do not adjust margins

ARTICLE

Ternary Alkali ion Thiogallates, A_5GaS_4 (A = Li and Na) with Isolated Tetrahedral Building Units and Their Ionic conductivity

Received 00th January 20xx,
Accepted 00th January 20xx

DOI: 10.1039/x0xx00000x

Srikanth Balijapelly,[a] Prashanth Sandineni,[a] Amit Adhikary,[a] Nikolay N. Gerasimchuk,[b] Aleksandr V. Chernatynskiy,[c] Amitava Choudhury [a, *]

Abstract: Two new ternary thiogallates in the series A_5GaS_4 (A = Li(**I**), Na(**II**)) have been synthesized for the first time employing gas passing route using oxide precursors and high temperature solid state route using stoichiometric combinations of elements, respectively. Li_5GaS_4 crystallizes in $P2_1/m$ space group and the structure is built up of layers of corner shared tetrahedra of LiS_4 and GaS_4 stacked along a-axis and the octahedrally coordinated Li ions residing in the interlayer space. Na_5GaS_4 crystallizes in *Pbca* space group and the structure consists of isolated $(GaS_4)^{5-}$ tetrahedra held together by charge balancing sodium ions in distorted tetrahedral and octahedral coordination geometries. Measurements of ionic conductivity of the compounds yielded the room temperature ionic conductivity of 1.8×10^{-7} and 4.0×10^{-7} S. cm^{-1} with activation energies of 0.54 and 0.28 eV, respectively, for **I** and **II**. Density functional theory calculations show close agreement in structural parameters with the measured data and predict the band gaps of 2.75 eV (**I**) and 2.70 eV (**II**). Single point hybrid functional calculations result in band gaps of 3.95 and 3.65 eV correspondingly, in better agreement with experimental values of ~4.1 eV for both. Bond valence landscape energy maps suggest absence of any suitable diffusion path for Li in Li_5GaS_4. On the other hand, BVEL maps of Na_5GaS_4 confirm that the tetrahedrally coordinated Na ions are responsible for ionic conduction, whereas involvement of octahedrally coordinated Na ions in the conduction process could not be discerned.

Introduction

Alkali ion containing ternary sulfides $A/M/Q$ (A = Li, Na, K, Rb, Cs; M = Main group metal, Q = S, Se, Te) possess wide structural and compositional varieties.[1-2] Various modes of connectivity between the chalcometallate building units lead to the formation of compounds with different dimensionality from non-van der Waal (vdW) layered, open framework type to isolated building units.[3-8] In recent years, these materials have attracted much attention because of their potential applications in solid electrolytes.[9] Highly conducting solid electrolyte would replace the flammable liquid electrolyte and impart greater safety.[9] Crystalline ternary thiophosphate, thioantimonnate and thiostannate based compounds in both lithium and sodium systems are currently extensively investigated for solid electrolyte applications.[3, 8 – 16] For example, high ionic conductivity at room temperature have been reported in some main-group metal chalcogenides as both Li- and Na-ion conductor, e.g., 6.4×10^{-4} S.cm^{-1} for $Li_{3.4}Si_{0.4}P_{0.6}S_4$,[10] and 2.2×10^{-3} S.cm^{-1} for $Li_{3.25}Ge_{0.25}P_{0.75}S_4$[11] and 1.2×10^{-2} S.cm^{-1} for $Li_{10}GeP_2S_{12}$[12]. Similarly in Na-ion conductors, ionic conductivity of 4.6×10^{-4} for Na_3PS_4,[13] 1×10^{-3} S.cm^{-1} for Na_3SbS_4[14] 4.0×10^{-3} S.cm^{-1} for $Na_{10}SnP_2S_{12}$[15] and 1.4×10^{-3} S.cm^{-1} for $Na_{11}Sn_2PS_{12}$ have been reported.[16] Though some of the oxide-based materials have shown superionic conductivity in Li- and Na-ion conduction, however, they require high sintering temperature to eliminate the effect of grain boundary and achieve high conductivity.[17] In the case of chalcogenide, movement of ions is more facile because of the weak interaction of ions with the highly polarizable chalcogen lattice.[18] More importantly, these chalcogenide materials can be cold pressed to achieve high conductivity because of the higher malleability of chalcogen lattice.[9]

Generally, these $A/M/Q$ compounds can be synthesized by solid state reaction of elements or by employing polychalcogenide reactive flux in sealed quartz tube. Besides solid-state syntheses, these days solution-based or mechanochemical syntheses are also becoming popular because of the need to prepare large quantities of materials in a simple manner for solid electrolyte applications.[19] However, among several $A/M/Q$ series of compounds, chalcogallate-based systems with simple building units are relatively less known, only a very small number of compositions exist to date.[4, 6, 20, 21] In the $A/Ga/Q$ (A = Li, Na; Q = S, Se) series the reported phases are $LiGaQ_2$ (Q = S, Se, Te),[6] $Na_6Ga_2Q_6$ (Q = S, Se)[20] and $Na_4Ga_2S_5$.[21] $LiGaQ_2$ adopts $NaFeO_2$ structure type with three-dimensional structure and are well-known NLO materials.[6] $Na_6Ga_2S_6$ has unique isolated edge shared GaS_4 tetrahedra forming $Ga_2Q_6^{6-}$ dimers whereas

[a]*Department of Chemistry, Missouri University of Science and Technology, Rolla, MO 65409, USA.*
[b]*Department of Chemistry, Missouri State University, Springfield, MO 65897, USA*
cDepartment of Physics, Missouri University of Science and Technology, Rolla, MO 65409, USA

Electronic Supplementary Information (ESI) available: The cif files of the compounds **I** and **II**. Tables showing atomic coordinates, equivalent isotropic and anisotropic displacement parameters for **I** and **II**. Figures of PXRD, TG-DSC, Li and Na-coordination and equivalent circuit for impedance fittings. See DOI: 10.1039/x0xx00000x

Please do not adjust margins

$Na_4Ga_2S_5$ possesses one dimensional chains of corner- and edge-shared GaS_4 tetrahedra.

Hence, we have directed our focus towards finding new phases in chalcogallate based systems in presence of both lithium and sodium ions. Towards this effort we have recently reported $NaGaS_2$, a non-vdW 2D solid with supertetrahedral building units showing unusual property of water absorption.[4] There is a good reason to investigate the formation of basic building unit of chalcogallate, such as tetrahedral, $[GaQ_4]^{5-}$ (Q = S, Se) for solid electrolyte since it will crystallize with five alkali ions. Besides favourable attributes of soft chalcogen atoms, presence of large number of ions should also play a pivotal role in facile ion conduction through the lattice. Further creation of defects in the lattice would inevitably create a good ionic conductor. However, to achieve this goal we first need to synthesize and structurally characterize the pristine and pure phase compounds made of basic building unit, A_5GaQ_4 (Q = S, Se). There are some reports of ionic conductivity measurements of Li_5GaS_4 and its solid solution with other main group elements,[22, 23] however, the crystal structure of Li_5GaS_4 is yet to be reported. To the best of our knowledge nothing is known about the Na-analogue, Na_5GaS_4. In this article, we report the synthesis, structure, and ionic conductivities of two new alkali ion containing non-isostructural thiogallates, Li_5GaS_4 (**I**) and Na_5GaS_4 (**II**), along with their theoretical band structures.

Experimental Section

Synthesis

Li_5GaS_4 (**I**) was initially synthesized from a reaction of stoichiometric mixture of 2.5 mmol of Li_2S, 1 mmol of Ga shavings, 1.5 mmol of S in a sealed quartz ampoule. The heating protocol used for this reaction involved heating to 700 °C at a rate of 30 °C/h, dwelling for 18h, and cooling down to room temperature at 35 °C/h. However, this route always yielded significant amounts of $LiGaS_2$ as the secondary phase along with Li_5GaS_4 (**I**) as the main phase (Figure S1). Hence, we opted for gas passing route through which a pure phase Li_5GaS_4 (**I**) was synthesized from 5 mmol of Li_2CO_3 and 1 mmol of Ga_2O_3 in a temperature-controlled tube furnace. The tube furnace was connected to a constant flow (20 sccm) of high purity argon carrier gas that passed through a tower of liquid carbon disulfide (CS_2) kept at room temperature. The vapours of CS_2 gas was carried over the oxide precursors for sulfidation at higher temperature. The temperature of the furnace was increased to 750 °C at a rate of 200 °C/h, after dwelling for 8 h, furnace was cooled to room temperature at a rate of 100 °C/h. Orange-red colour crystalline product was formed (Figure S2). The obtained product was ground again using a mortar pestle after transferring it inside an argon filled glovebox and subjected to a second cycle of heating in order to achieve phase pure compound. After the reaction very stable homogenous product containing orange-red colour crystals were transferred to an argon filled glove box (O2 < 0.1ppm). Na_5GaS_4 (**II**) was synthesized by reacting stoichiometric mixture of 2.5 mmol of Na_2S, 1 mmol of Ga shavings, 1.5 mmol of S in a sealed quartz ampoule. The sealed ampoule was heated in a temperature-controlled furnace and the temperature was ramped to 600 °C at a rate of 25 °C/h, after dwelling for 96 h, the furnace was cooled down to room temperature at 30 °C/h rate. Pale orange colour crystals were recovered after breaking the ampoule in an argon-filled glove box (Figure S2). Appropriate crystals were used for single crystal X-ray diffraction and finely ground powder samples were used for other characterizations including powder X-ray diffraction.

X-Ray crystallography

Good quality crystals were chosen for single crystal X-Ray diffraction on a Bruker smart apex diffractometer equipped with a sealed tube X-ray source of Mo–Kα radiation (λ = 0.71073 Å). Room temperature or –53 °C diffraction data sets were collected using SMART[24] software with a step of 0.3° in ω scan and 20 s or 10 s/frame exposure time, respectively, for **I** and **II**. Programs SAINT[25] and SADABS[25] were used for the data integration and absorption correction, respectively. SHELXS-97 and difference Fourier syntheses were used to solve the structures.[26] Full-matrix least-squares refinement against $|F^2|$ was carried out using the SHELXTL-PLUS suite of programs.[25] Li_5GaS_4 crystallized in $P2_1/m$ space group while the Na-analogue, Na_5GaS_4, crystallized in *Pbca* space group. All the atoms can be easily located from the difference Fourier maps and weighted R factor, wR_2 converged to a low value without leaving any unaccounted electron density. Final refinements including the refinements of anisotropic thermal parameters were performed using SHELX-2018 incorporated in ShelXLe.[27] Crystal data and final refinement parameters are given in Table **1** and selected bond lengths are given in Table **2** for compounds **I** and **II**. Atomic coordinates along with their isotropic thermal parameters are given in SI (Tables S1 and S2).

Table 1. Crystal data and refinement details of **I** and **II**

Compounds	**I**	**II**
Empirical formula	Li_5GaS_4	Na_5GaS_4
Formula weight	232.66	312.91
Temperature	300(2) K	220(2) K
Wavelength	0.71073 Å	0.71073 Å
Crystal system	Monoclinic	Orthorhombic
Space group	$P2_1/m$	*Pbca*
Unit cell dimensions	a = 6.2711(18) Å	a = 12.045(15) Å
	b = 7.864(2) Å	b = 7.0212(9) Å
	c = 6.8610(19) Å	c = 21.535(3) Å
	β = 90.118(4)°	
Volume	338.36(16) Å^3	1821.3(4) Å^3
Z	2	8
Density (calculated)	2.284 g/cm^3	2.282 g/cm^3
Absorption coefficient	5.166 mm^{-1}	4.089 mm^{-1}
Goodness-of-fit on F^2	1.091	1.059
R [$I > 2\sigma(I)$]	R_1 = 0.0426	R_1 = 0.0290
wR (F^2) (all data)	wR_2 = 0.1083	wR_2 = 0.0733

[a] $R_1 = \sum||F_o| - |F_c|/\sum|F_o|$.

This journal is © The Royal Society of Chemistry 20xx

[b]$wR_2 = \{\sum[w(F_o^2 - F_c^2)^2]/\sum[w(F_o^2)^2]\}^{1/2}$, $w = 1/[\sigma^2(F_o)^2 + (aP)^2 + bP]$, where $P = [F_o^2 + 2F_c^2]/3$

Table 2: Selected bond lengths (Å) of compounds **I** and **II**.

Li_5GaS_4 (**I**)		Na_5GaS_4 (**II**)	
Ga1 – S3$^{\#1}$	2.2608(17)	Ga1 – S2$^{\#1}$	2.2758(11)
Ga1 – S1	2.2729(12)	Ga1 – S1$^{\#2}$	2.2778(11)
Ga1 – S1$^{\#2}$	2.2730(12)	Ga1 – S4	2.2834(11)
Ga1 – S2	2.2773(16)	Ga1 – S3$^{\#3}$	2.2852(11)

I: $^{\#1}$ x, -y + 1/2, z; $^{\#2}$ x, -y + 1/2, z; **II**: $^{\#1}$ x, y – 1, z; $^{\#2}$ -x + 1/2, y – 1/2, z; $^{\#3}$ -x + 1, -y + 1, -z + 1.

Powder X-ray diffraction

The laboratory powder pattern was collected from a PANalytical X'Pert Pro diffractometer equipped with a Cu Kα anode and a linear array PIXcel detector over a 2θ range of 5 to 90° with an average scanning rate of 0.0472° s^{-1}. As-synthesized, hand ground samples were loaded into an airtight cell covered with the kapton film to collect the PXRD pattern (Figure 1).

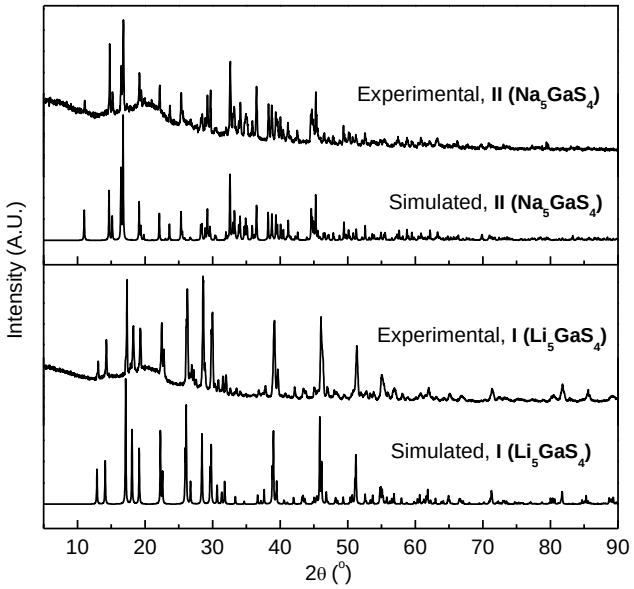

Figure 1. Comparison of simulated and experimental powder X-ray diffraction patterns for compounds, **I** and **II**. The broad hump between 2θ = 15 to 25 is due the Kapton film.

DRS measurements

Diffuse reflectance measurements for compounds **I** and **II** were performed in Labsphere's integrating sphere (Model DRA-CA-30I) fitted on a Varian CARY 100 Bio UV-Vis spectrophotometer. A Spectralon's white standard was used as a 100% reflectance standard. The Kubelka–Munk function was used to transform the reflectance into absorption.[28] $h\nu$ *vs* $(\alpha h\nu)^2$ plots (Figure 2) show flat region parallel to X–axis followed by a steep jump due to the electronic transition from valence band to the conduction band. The band gap was determined by the intersection of the extrapolated flat and steep regions of the plot. The band gap values obtained for compounds **I** and **II** are almost similar and close to ~4.1 eV.

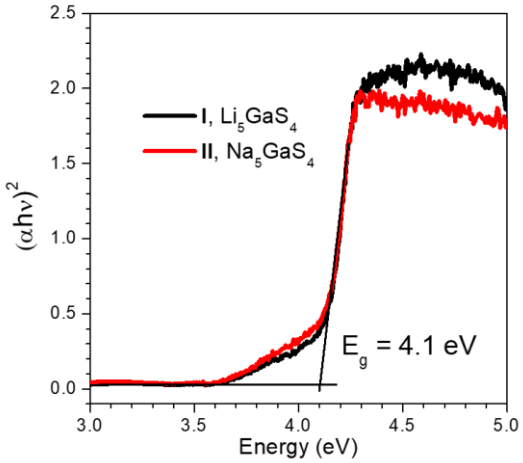

Figure 2. Diffuse reflectance plot for compounds **I** and **II**.

Thermal analysis

Simultaneous TGA, DSC experiments were performed on TA Instruments Q50 TGA and Q600 SDT for compounds **I** and **II** from room temperature to 900 °C with a scan rate of 10 °C/min under high purity argon gas. Samples of *ca* 20 mg weight was placed into brand new calcined alumina crucible for the experiment. The plots are presented in SI (Figure S3). The TGA and DSC plots show endothermic events occurring at 837 °C for compound **I** and 670 °C for compound **II**, which could be due to melting of the compounds. However, the phase changes were not very sharp because of the weight loss of ~1.3 % after 300 °C due to reaction with oxygen impurities present in the inert gas as these TG-DSCs were performed in unsealed open alumina cups. In fact, it is practically impossible to eliminate traces of air adsorbed on the Q600 analyzer interior surfaces of horizontal furnace even after ~20 min of the UHP-grade argon flow of 100±2 mL/min. However, it is evident that both compounds **I** and **II** are thermally stable at least up to 650 °C. Powder patterns of the remaining sample residues after TGA-DSC experiments (Figure S4) did not show any phase changes as both the samples retained the original crystal structure.

Impedance measurements

AC impedance measurements were performed from 1Hz to 1MHz using Biologic instruments SP-150 impedance analyzer with an AC signal amplitude of 500 or 100 mV. The hand ground samples were cold pressed applying a force of 280 MPa in a stainless-steel pressing die inside an argon filled glove box (O_2 < 0.1 ppm). Indium foil was used as the blocking electrodes. The pellets were placed in an airtight Swagelok type cell and heated in a temperature-controlled box furnace to measure the

temperature dependence of the ionic conductivity. The impedance data were collected at every 10 °C increment by keeping the temperature of each measurement constant for at least an hour to reach the thermal equilibrium.

DFT Calculations

We carried out investigation of the structural and electronic properties of both compounds using Density Functional Theory (DFT) as implemented in VASP computational package.[29-32] We employed the revised Perdew-Burke-Ernzerhof generalized gradient approximation (PBESol) to the density functional[33] and used Projected Augmented Wave (PAW) pseudopotential to describe the effect of the core electrons. Energy cut off for all calculations is 500 eV, while Brillouin zone integration used Monkhorst-Pack[34] k-point grid with dimensions of 5x5x5 for compound **I** and 3x3x3 for compound **II**.

Results and Discussion

Structural description

Though compositionally both compounds **I** and **II** are similar, structurally they are different. Compound **I** crystallizes in a centrosymmetric monoclinic, $P2_1/m$ space group and is isostructural with Na_5InS_4,[35] Li_5AlS_4.[36] The asymmetric unit consists of three sulfur atoms, one gallium, and four lithium atoms (Figure 3a). Li1 and S1 occupy general positions on 4*f* Wyckoff site, while one gallium atom, two sulfur atoms (S2 and S3), and two lithium atoms (Li2 and Li3) are located on special positions denoted as 2*e* Wyckoff site. One remaining lithium atom (Li4) is also located on a special position, 2*a* Wyckoff site. Li1 and Li3 adopt distorted tetrahedral coordination while Li2 and Li4 adopt distorted octahedral coordination (Figure 3b and Figure S5). The structure of compound **I** can be described as hexagonal close packing of anions which are stacked along the *a*-axis in *ABAB* fashion. Such stacking of S creates eight tetrahedral holes and four octahedral holes of which 3/8th of tetrahedral holes are filled with Li (Li1, Li3) and Ga cations and ½ of octahedral voids are filled with Li (Li2 and Li4). However, they differ in the manner of occupancy of tetrahedral and octahedral sites. The pair of close-packed (CP) layer (Figure 3c) in which only tetrahedral holes are occupied alternate between CP layers in which only the octahedral holes are occupied as shown in Figure 3b. Alternatively, the structure can be viewed as a layered type with layers formed by corner shared tetrahedral network of LiS_4 (Li1 and Li3) and GaS_4 stacked along *a*-axis where the interlayer space is occupied by octahedrally coordinated Li-ions (Li2 and Li4) (Figure 3b). Li – S bond distances are in the range of 2.398(11) – 2.558(13) Å for tetrahedrally coordinated Li atoms (Li1, Li3) and 2.6562(11) – 3.040(12) Å for octahedrally coordinated Li atoms (Li2, Li4) which are in good agreements with other lithium containing main group sulfide, such as lithium thioalluminate, Li_5AlS_4.[36] Na_5GaS_4 (**II**) crystallizes in orthorhombic *Pbca* space group with asymmetric unit containing five sodium atoms, one gallium atom, and four sulfur atoms and all the atoms are in the general positions, 2*e* Wyckoff site (Figure 3d). Na_5GaS_4 adopts

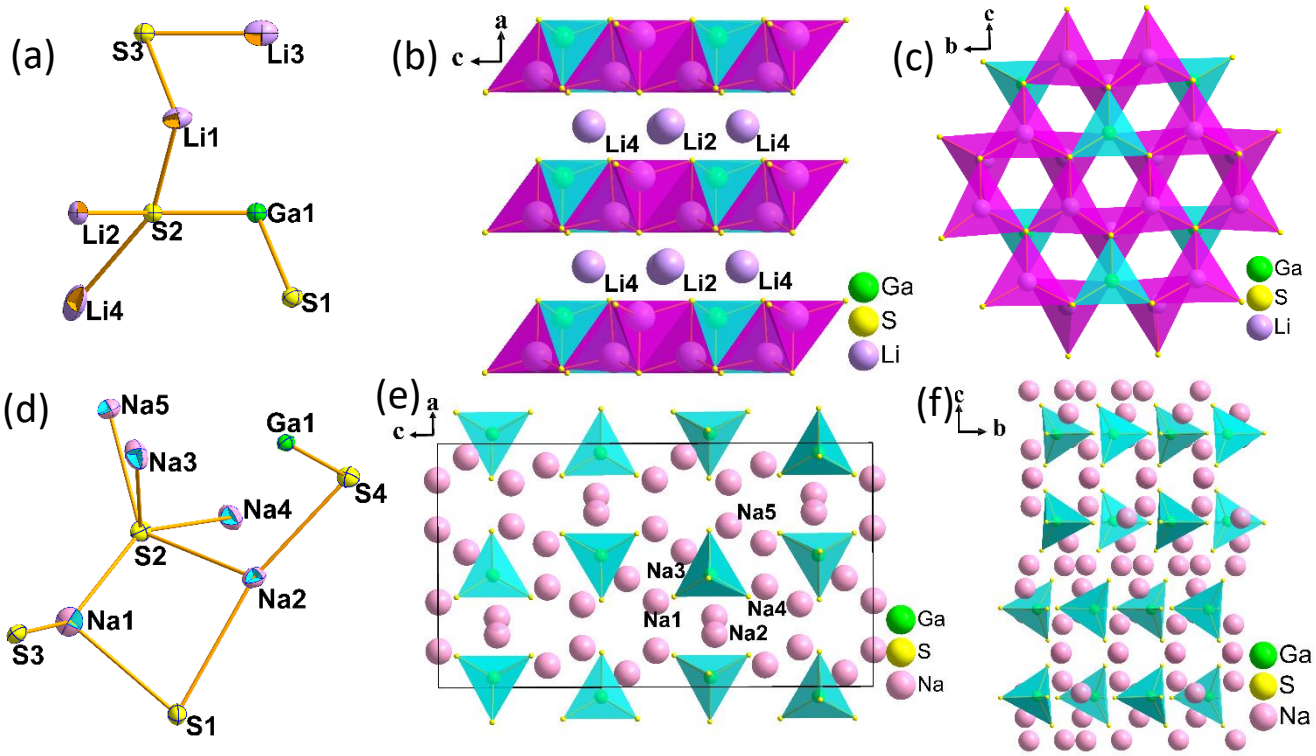

Figure 3. (a) Asymmetric unit of compound **I**. (b) Layers formed by GaS_4^{5-} and tetrahedrally coordinated Li stacked along *a*-axis where the interlayer space is occupied by octahedrally coordinated Li2 and Li4. (c) Polyhedral view of the layer, in which 3/8th of the tetrahedral voids are filled by Ga1, Li1 and Li3. (d) Asymmetric unit of compound **II**. (e) Unit cell showing the isolated GaS_4^{5-} tetrahedral units, separated by charge balancing sodium ions (f) Zig-zag arrangement of GaS_4^{5-} tetrahedral units along *b*-axis. (Thermal ellipsoids are given at 40 % probability.)

This journal is © The Royal Society of Chemistry 20xx

Please do not adjust margins

Na_5FeO_4[37] structure type and isostructural with Na_5AlS_4.[38] The structure of **II** composed of isolated GaS_4^{5-} tetrahedra with charge balancing sodium ions adopting distorted tetrahedral (Na1, Na3, Na4, and Na5) and distorted octahedral (Na2) coordination, respectively (Figure 3e and Figure S6). Columns of isolated GaS_4 tetrahedral building units are aligned along *b*-axis and are related by two-fold screw axis (Figure 3f). Na – S bond distances are in the range of 2.6861(19) – 2.952(2) and 2.8300(18) – 3.2360(18) Å for tetrahedrally and octahedrally coordinated Na atoms, respectively, which are in good agreement with isostructural sodium based thioalluminate Na_5AlS_4.[38] It is interesting to note here that many of the ternary compounds in the *A/M/*S series (e.g., Li_4GeS_4 or Li_4SnS_4) are moisture sensitive.[39] Though compound Na_5GaS_4 (**II**) is found to be reasonably stable in air for few hours, the compound Li_5GaS_4 (**I**) turned out to be very stable (four to five days), which could be attributed to the 2-dimensional network of LiS_4 and GaS_4.

Here, it should be noted that though the compounds with general formula A_5MQ_4 (*A* = Li, Na; *M* = Al, Ga, In; *Q* = S, Se) are compositionally similar, they adopt different structure types. This may be due to differences in sizes between the alkali ions and the main group metal ion. Among the compositions that exist in A_5MQ_4 family, for example Na_5InS_4[35] and Li_5AlS_4[36] are isostructural to **I** and crystallize in $P2_1/m$ space group with layered structure. Similarly, Na_5AlS_4[38] and **II** are isostructural and crystallize in *Pbca* space group containing isolated GaS_4 tetrahedral units. Increasing the size of alkali ion from Na to K as in K_5GaSe_4, it is still found to crystallize in *Pbca* space group similar to **II** containing isolated $GaSe_4$ tetrahedra but possesses much larger unit cell volume.[40] However, recently reported K_5InSe_4 adopts a new structure type crystallizing in *C*2/*c* space group.[41]

Theoretical calculations

Starting from the experimentally elucidated structures, we first performed structural relaxation until the maximum force on the atoms was less than 10^{-2} eV/Å. Relaxed structures show excellent agreement with experiment. For both compounds, the volume of the theoretical structure is slightly smaller than experimentally observed one, by 10 and 23 Å^3 correspondingly.

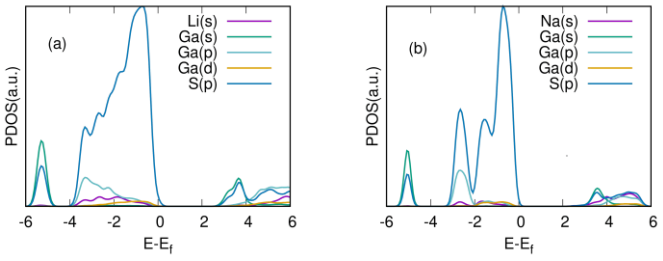

Figure 4. Projected electronic density of states in (a) Li_5GaS_4(**I**) and (b) Na_5GaS_4 (**II**).

The calculated projected density of states for Li_5GaS_4 (**I**) and Na_5GaS_4 (**II**) are shown in Figure 4 (a and b). The calculated band gaps for **I** and **II** are 2.75 and 2.69 eV, respectively. Considering the typical underestimation of band gaps by the conventional DFT, we also carried out the single point calculations with the HSE06 hybrid functional,[42] which typically improves the predictions for band gap. Due to the computational load, lesser number of the k-points were used of the Brillouin zone integration: 2x2x2 for the compound **I** and gamma-point only for **II**. This calculation predicted band gaps of 3.95 and 3.65 eV correspondingly, in much better agreement with experiment (~4.1 eV). As illustrated in Figure 4a and 4b, projected density of states for both the compounds share some similarity in the contribution to the valence and conduction bands. The states below the Fermi level are dominated by S 3*p* states in both the compounds. The conduction band minimum (CBM) has the major contribution from S 3*p* states and Ga 4*s* states. There is no predominant contribution from alkali ion states to the valence band suggesting minimal covalent interactions with the alkali ions. It is still interesting to observe the difference in the calculated band gap of the two materials by the HSE06 functional considering both have the isolated GaS_4^{5-} unit mainly contributing to the bands around the energy gap and not the alkali ions. Therefore, the differences may come from the indirect effect of alkali ions and differences of packing of the GaS_4^{5-} units in the unit cell since **I** and **II** are not isostructural.

Ionic Conductivity

AC impedance measurements were performed to calculate the ionic conductivity and activation energies. The Nyquist plots for the compounds **I** and **II** are shown in Figures 5 (a) and (b) consist of a high frequency semicircle and a low frequency tail corresponding to bulk resistance and charge accumulation at the blocking electrode. The equivalent circuit used, and the related fitting parameters for room temperature ionic conductivity are detailed in the SI (Figure S7). Ionic conductivity was calculated from the bulk resistance extracted from complex impedance plots. Temperature dependent ionic conductivity was measured from room temperature to 75 °C at every 10 °C interval to calculate the activation energy. Within the measured range the ionic conductivities both compounds follow Arrhenius behaviour. The activation energies were calculated using $\sigma_T = \sigma_o \exp(-E_a/k_BT)$ where σ_T is the ionic conductivity, σ_o is a pre-exponential factor, T is the absolute temperature, and k_B is the Boltzmann constant. The room temperature ionic conductivities are 1.8×10^{-7} S.cm^{-1} for Li_5GaS_4 (**I**) and 4.0×10^{-7} S.cm^{-1} for Na_5GaS_4 (**II**). The calculated activation energies for compounds **I** and **II** are 0.54 and 0.28 eV, respectively. Despite having almost similar ionic conductivity in compounds **I** and **II**, there exist significant difference in the activation energies, which could arise due to different conduction mechanisms. Generally, a concerted type mechanism in which multiple adjacent ions simultaneously hop to neighbouring equilibrium site gives rise to low activation barriers compared to single ion hopping.[43] BVEL (Bond Valence Energy Landscapes) were calculated to find out the most probable minimum energy trajectories for the Li and Na ions. Deviations in the Bond Valence Sum can be correlated to the possible ionic conduction path in the lattice. These deviations can be plotted as an isosurface using VESTA.[44] Bond valence energy landscape maps are plotted as an isosurface energy levels $|\Delta V|$ = 0.3, 0.5, 0.7 v.u for compounds **I** (Figure 6 a, b, c) and **II** (Figure 6 d, e, f) . No suitable path for ion percolation was found for compound Li_5GaS_4 (**I**), which could be the reason for low ionic conductivity and high activation energy.

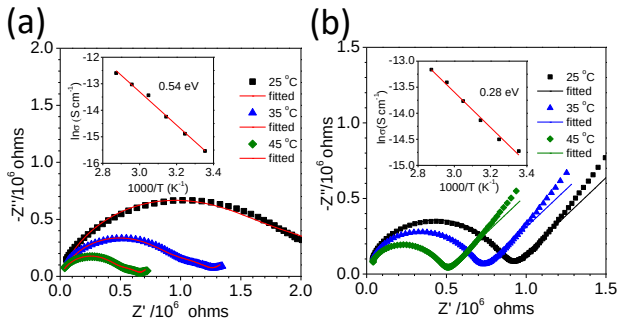

Figure 5. Nyquist plot for ionic conductivity of (a) Compound **I** (Li_5GaS_4) (b) Compound **II** (Na_5GaS_4). Inset shows the activation energy calculated from experimentally measured ionic conductivity versus temperature. Dots represents the experimental ionic conductivity and dashed line represents the Arrhenius fit to the data.

The ionic conductivity of Li_5GaS_4 is much higher than the corresponding Al-analogue, Li_5AlS_4 (σ_{RT} = 9.73 × 10^{-9} S.cm^{-1}),[36] however, comparable to many related Li based ternary sulfide compounds, such as Li_4GeS_4 (σ_{RT} = 2.0×10^{-7} S.cm^{-1}),[22] but somewhat lower than Li_4SnS_4 (σ_{RT} = 7 × 10^{-5} S.cm^{-1})[8] and Li_2SnS_3 (σ_{RT} = 1.5 × 10^{-5} S.cm^{-1}).[3] Na_5GaS_4 has the room temperature ionic conductivity of 4.0 ×10^{-7} S.cm^{-1} which is slightly better than isostructural Al-analogue, Na_5AlS_4 (σ_{RT} = 1.64×10^{-7} S.cm^{-1}).[38] Slightly improved ionic conductivity of Na_5GaS_4 compared to Na_5AlS_4 could be due to larger ionic radii of Ga^{3+} compared to Al^{3+}. For Na_5GaS_4, a two-dimensional diffusion path was observed from BVEL calculation. BVEL map also confirms that Na2, which is in distorted octahedral coordination does not take part in the ion conduction. Similar observation has been found for isostructural Na_5AlS_4.[38]

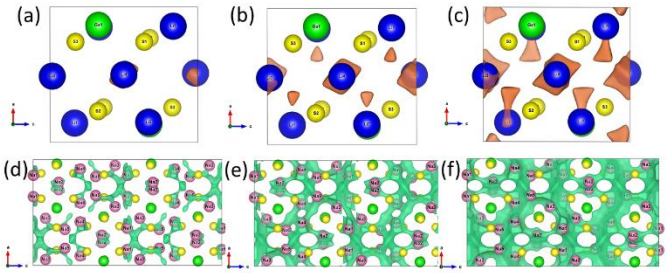

Figure 6. Bond valence sum (|ΔV|) maps of compound **I** at an isosurface $|\Delta V| = 0.3\ v.u.$ figure (a), $0.5\ v.u.$ figure (b) $0.7\ v.u.$ figure (c) and for compound **II** $|\Delta V| = 0.3\ v.u.$ figure (d), $0.5\ v.u$ figure (e), $0.7\ v.u$ figure (f).

Solid solutions with aliovalent substitutions would create Li/Na vacancies which is an important prerequisite for superionic conductors. Recently, Bernhard et al. reported that solid solutions in $Li_{4.4}M_{0.4}M'_{0.6}S_4$ (M = Al^{3+}, Ga^{3+}, and M' = Ge^{4+}, Sn^{4+}) series not only create vacancies, but also altered the arrangement of tetrahedral metal sites, with novel ordered and disordered lithium combination.[23] Harm et al. reported a solid solution series of $Na_{5-x}Al_{1-x}Si_xS_4$ ($0 \le x \le 1$) and emergence of double salt $Na_9(AlS_4)(SiS_4)$ in the composition range of $0.5 \le x \le 0.75$ with high alkali ion concentration with versatile Na-coordination.[36] However, it will be interesting to substitute some percentage of Li/Na with transition metal, in which case one can perform oxidative de-insertion of alkali ion from the host lattice to create more defects. Li_5GaS_4 would be an ideal candidate for substitution with transition metal due to its 2D layered structure. Substitution of pentavalent metal ions (P^{+5}, Sb^{+5}) in the Ga-site can also be investigated in A_5GaS_4 (A = Li, Na) to create more defects for improving the ionic conductivity. With the report of structures of pristine A_5GaS_4 (A = Li, Na) in this article, it will be much easier to investigate the structural changes as a function of dopant.

Conclusions

We have successfully synthesized two new ternary thiogallates containing alkali ions and determined their structures. Though both are compositionally similar but adopt different crystal structures. This work also proves that gas passing reactions would give access to new phases which may not be accessible through typical solid-state reactions from the elements. Ionic conductivity measurements along with BVEL calculations suggest no diffusion paths in Li_5GaS_4 and 2D diffusion paths in Na_5GaS_4 exists at moderate activation energies. DFT calculations show that both the compounds are wide band-gap semiconductors with optical bandgaps > 2.5 eV and no significant contribution was found from Li/Na states to the conduction and valence band indicating predominant ionic interactions with the alkali metal ions. Currently we are investigating doping of hypervalent metal ions to induce vacancies in the lattice to improve the ionic conductivity.

Author Contributions

AC conceived the problem and supervised the work. PS, SB, and AA carried out the synthesis and measured ionic conductivity. NG helped with thermal analysis and experimental band gap determination. AVC performed the band structure calculations. AC and SB wrote the manuscript and all the authors approved the manuscript and gave feedback.

Conflicts of interest

There are no conflicts to declare.

Acknowledgements

The authors acknowledge the funding from National Science Foundation (DMR- 1809128). This work was supported in part by the National Science Foundation under Grant No. OAC-1919789.

Notes and references

1 W. S. Sheldrick and M. Wachhold, *Coord. Chem. Rev.*, 1998, **176**, 211–322.

2 S. Dehnen and M. Melullis, *Coord. Chem. Rev.*, 2007, **251**, 1259–1280.

This journal is © The Royal Society of Chemistry 20xx

Please do not adjust margins

3 J. A. Brant, D. M. Massi, N. A. W. Holzwarth, J. H. Macneil, A. P. Douvalis, T. Bakas, S. W. Martin, M. D. Gross and J. A. Aitken, *Chem. Mater*., 2015, **27**, 189–196.

4 A. Adhikary, H. Yaghoobnejad Asl, P. Sandineni, S. Balijapelly, S. Mohapatra, S. Khatua, S. Konar, N. Gerasimchuk, A. V. Chernatynskiy and A. Choudhury, *Chem. Mater*., 2020, **32**, 5589–5603.

5 F. Alahmari, B. Davaasuren, A. H. Emwas and A. Rothenberger, *Inorg. Chem*., 2018, **57**, 3713–3719.

6 L. Isaenko, A. Yelisseyev, S. Lobanov, A. Titov, V. Petrov, J.-J. Zondy, P. Krinitsin, A. Merkulov, V. Vedenyapin and J. Smirnova, *Cryst. Res. Technol*., 2003, **38**, 379–387.

7 S. Huber, C. Preitschaft, R. Weihrich and A. Pfitzner, Z. Anorg. Allg. Chem., 2012, **638**, 2542–2548.

8 T. Kaib, P. Bron, S. Haddadpour, L. Mayrhofer, L. Pastewka, T. T. Jä Rvi, M. Moseler, B. Roling and S. Dehnen, Chem. Mater., 2013, 25, 2961 —2969.

9 Z. Zhang, Y. Shao, B. Lotsch, Y. S. Hu, H. Li, J. Janek, L. F. Nazar, C. W. Nan, J. Maier, M. Armand and L. Chen, *Energy Environ. Sci*., 2018, **11**, 1945–1976.

10 M. Murayama, R. Kanno, M. Irie, S. Ito, T. Hata, N. Sonoyama and Y. Kawamoto, *J. Solid State Chem*., 2002, **168**, 140–148.

11 R. Kanno and M. Murayama, *J. Electrochem. Soc*., 2001, **148**, A742.

12 N. Kamaya, K. Homma, Y. Yamakawa, M. Hirayama, R. Kanno, M. Yonemura, T. Kamiyama, Y. Kato, S. Hama, K. Kawamoto and A. Mitsui, *Nat. Mater*., 2011, **10**, 682–686.

13 A. Hayashi, K. Noi, N. Tanibata, M. Nagao and M. Tatsumisago, *J. Power Sources*, 2014, **258**, 420–423.

14 H. Wang, Y. Chen, Z. D. Hood, G. Sahu, A. S. Pandian, J. K. Keum, K. An and C. Liang, *Angew. Chemie Int. Ed*., 2016, **55**, 8551–8555.

15 W. D. Richards, T. Tsujimura, L. J. Miara, Y. Wang, J. C. Kim, S. P. Ong, I. Uechi, N. Suzuki and G. Ceder, *Nat. Commun*., 2016, **7**, 1–8.

16 Z. Zhang, E. Ramos, F. Lalère, A. Assoud, K. Kaup, P. Hartman and L. F. Nazar, *Energy Environ. Sci*., 2018, **11**, 87–93.

17 K. B. Hueso, M. Armand and T. Rojo, *Energy Environ. Sci*., 2013, **6**, 734–749.

18 A. Sakuda, A. Hayashi and M. Tatsumisago, *Sci. Rep*., 2013, **3**, 1–5.

19 S. Boulineau, M. Courty, J. M. Tarascon and V. Viallet, *Solid State Ionics*, 2012, **221**, 1–5.

20 B. Eisenmann and A. Hofmann, *Z. Kristallogr. NCS*., 1991, **197**, 147–148.

21 K. O. Klepp, *Z. Naturforsch*., 1992, **47b**, 937

22 R. Kanno, T. Hata, Y. Kawamoto and M. Irie, *Solid State Ionics*, 2000, **130**, 97–104.

23 B. T. Leube, K. K. Inglis, E. J. Carrington, P. M. Sharp, J. F. Shin, A. R. Neale, T. D. Manning, M. J. Pitcher, L. J. Hardwick, M. S. Dyer, F. Blanc, J. B. Claridge and M. J. Rosseinsky, *Chem. Mater*., 2018, **30**, 7183–7200.

24 Bruker- SMART. Bruker AXS Inc., Madison, Wisconsin, USA. 2002.

25 Bruker-SAINT and SADABS, and SHELXTL. Bruker AXS Inc., Madison, Wisconsin, USA, 2008

26 G. M. Sheldrick, Acta Crystallogr. Sect. A Found. *Crystallogr*., 2008, **64**, 112–122.

27 C. B. Hübschle, G. M. Sheldrick and B. Dittrich, *J. Appl. Crystallogr*., 2011, **44**, 1281–1284.

28 P. Kubelka and F. Z. Munk, *Tech. Phys*., 1931, **12**, 593–601.

29 G. Kresse and J. Hafner, *Phys. Rev. B*, 1993, **47**, 558–561.

30 G. Kresse and J. Furthmüller, *Comput. Mater. Sci*., 1996, **6**, 15–50.

31 G. Kresse and J. Furthmüller, *Phys. Rev. B - Condens. Matter Mater. Phys*., 1996, **54**, 11169–11186.

32 D. Joubert, *Phys. Rev. B - Condens. Matter Mater. Phys*., 1999, **59**, 1758–1775.

33 J. P. Perdew, A. Ruzsinszky, G. I. Csonka, O. A. Vydrov, G. E. Scuseria, L. A. Constantin, X. Zhou and K. Burke, *Phys. Rev. Lett*., 2008, **100**, 136406.

34 H. J. Monkhorst and J. D. Pack, *Phys. Rev. B*, 1976, **13**, 5188–5192.

35 B. Eisenmann and A. Hofmann, *Z. Kristallogr. NCS*., 1991, **197**, 169–170.

36 H. Lim, S. C. Kim, J. Kim, Y. Il Kim and S. J. Kim, *J. Solid State Chem*., 2018, **257**, 19–25.

37 G. Brachtel and R. Hoppe, *Z. Anorg. Allg. Chem*., 1978, **446**, 77–86.

38 S. Harm, A.-K. Hatz, C. Schneider, C. Hoefer, C. Hoch and B. V. Lotsch, *Front. Chem*., 2020, **8**, 90.

39 J. H. Macneil, D. M. Massi, J. H. Zhang, K. A. Rosmus, C. D. Brunetta, T. A. Gentile and J. A. Aitken, *J. Alloys Compd*., 2014, **586**, 736–744.

40 B. Eisenmann and A. Hofmann, *Z. Kristallogr. NCS*., 1991, **197**, 163–164.

41 M. Langenmaier, S. Wissinger and C. Röhr, Z. *Anorg. Allg. Chem.*, 2020, **646**, 1545–1554.

42 A. V. Krukau, O. A. Vydrov, A. F. Izmaylov and G. E. Scuseria, *J. Chem. Phys*., 2006, **125**, 224106.

43 X. He, Y. Zhu and Y. Mo, *Nat. Commun*., 2017, **8**, 1–7.

44 K. Momma and F. Izumi, *J. Appl. Crystallogr*., 2011, **44**, 1272–1276.

This journal is © The Royal Society of Chemistry 20xx